Bioactive Materials 2 (2017) 208–223

Contents lists available at ScienceDirect

Bioactive Materials

journal homepage: http://www.keaipublishing.com/en/journals/bioactive-materials/

Analysis of the *in vitro* degradation and the *in vivo* tissue response to bi-layered 3D-printed scaffolds combining PLA and biphasic PLA/bioglass components – Guidance of the inflammatory response as basis for osteochondral regeneration

Mike Barbeck [a, 1], Tiziano Serra [b, 2, 1], Patrick Booms [c], Sanja Stojanovic [d], Stevo Najman [d], Elisabeth Engel [b, e, f], Robert Sader [c], Charles James Kirkpatrick [c], Melba Navarro [b, **, 3], Shahram Ghanaati [c, *]

[a] Private Office, Berlin, Germany
[b] Institute for Bioengineering of Catalonia (IBEC), Biomaterials for Regenerative Medicine, Barcelona, Spain
[c] Clinic of Oro-Maxillofacial and Plastic Surgery, FORM-Lab, Goethe University Frankfurt, Frankfurt, Germany
[d] University of Niš, Faculty of Medicine, Department for Cell and Tissue Engineering, Institute of Biology and Human Genetics, Niš, Serbia
[e] Technical University of Catalonia (UPC), Dpt. Materials Science and Metallurgy, Spain
[f] CIBER en Bioingenieria, Biomateriales y Nanomedicina (CIBER-BBN), Spain

ARTICLE INFO

Article history:
Received 25 November 2016
Received in revised form
13 June 2017
Accepted 13 June 2017
Available online 23 June 2017

Keywords:
Bioactive glass
Polylactic acid (PLA)
Bi-layer scaffold
Multinucleated giant cells
Bone substitute
Vascularization
Calcium phosphate glass

ABSTRACT

The aim of the present study was the *in vitro* and *in vivo* analysis of a bi-layered 3D-printed scaffold combining a PLA layer and a biphasic PLA/bioglass G5 layer for regeneration of osteochondral defects *in vivo* Focus of the *in vitro* analysis was on the (molecular) weight loss and the morphological and mechanical variations after immersion in SBF. The *in vivo* study focused on analysis of the tissue reactions and differences in the implant bed vascularization using an established subcutaneous implantation model in CD-1 mice and established histological and histomorphometrical methods.

Both scaffold parts kept their structural integrity, while changes in morphology were observed, especially for the PLA/G5 scaffold. Mechanical properties decreased with progressive degradation, while the PLA/G5 scaffolds presented higher compressive modulus than PLA scaffolds. The tissue reaction to PLA included low numbers of BMGCs and minimal vascularization of its implant beds, while the addition of G5 lead to higher numbers of BMGCs and a higher implant bed vascularization. Analysis revealed that the use of a bi-layered scaffold shows the ability to observe distinct *in vivo* response despite the physical proximity of PLA and PLA/G5 layers.

Altogether, the results showed that the addition of G5 enables to reduce scaffold weight loss and to increase mechanical strength. Furthermore, the addition of G5 lead to a higher vascularization of the implant bed required as basis for bone tissue regeneration mediated by higher numbers of BMGCs, while within the PLA parts a significantly lower vascularization was found optimally for chondral regeneration. Thus, this data show that the analyzed bi-layered scaffold may serve as an ideal basis for the regeneration of osteochondral tissue defects. Additionally, the results show that it might be able to reduce the number

* Corresponding author. FORM-Lab, Department for Oral, Cranio-Maxillofacial and Facial Plastic Surgery Medical Center of the Goethe University Frankfurt, Theodor-Stern-Kai 7, Building 23B, UG 60596, Frankfurt/Main, Germany.
** Corresponding author. International Center for Numerical Methods in Engineering (CIMNE), Edificio Nexus (103), Carrer del Gran Capità, 2-4, 08034, Barcelona, Spain.
E-mail addresses: melba.navarro@gmail.com (M. Navarro), shahram.ghanaati@kgu.de (S. Ghanaati).
Peer review under responsibility of KeAi Communications Co., Ltd.
[1] The authors contributed equally.
[2] On leave to AO Research Institute Davos, Switzerland.
[3] On leave to the International Center for Numerical Methods in Engineering (CIMNE), Barcelona, Spain.

http://dx.doi.org/10.1016/j.bioactmat.2017.06.001

of experimental animals required as it may be possible to analyze the tissue response to more than one implant in one experimental animal.

1. Introduction

The regeneration of osteochondral tissue defects after traumata or resections is a major clinical challenge. In this context, different healing mechanisms for these both tissues – although both tissues are in close proximity such as in case of joints – have been described [1]. The main differences in the regeneration processes of bone and articular cartilage is the need for vascularization [1–3]. In case of bone tissue, a high vascularization is a basic factor for its regeneration as it permits the transport of nutrients, *e.g.* oxygen, to the defect sides [3]. It has been shown that a high expression of vascular endothelial growth factor (VEGF) and a related high implant bed vascularization but also direct effects of this molecule enable to increase the bone healing process [2,3]. In contrast, the regeneration of articular cartilage is not dependent on a high blood support as it is a relatively avascular tissue including a hypoxic milieu [4].

In the last decades, many different substitute materials for both bone and cartilage repair were developed that should allow simultaneous regeneration of both tissues while becoming resorbed over time. In case of bone substitutes, one aim of these new materials was even to increase the implant bed vascularization and, thus, their regenerative potential. Interestingly, the incorporation of VEGF into different bone substitutes has been tested but this combination has not been established as a real clinical alternative until know based on different reasons such as the high costs, the very short half-life of this molecule and the lack of knowledge about the (individual) concentration of this growth factor [2,5]. Furthermore, different concepts combining bone substitutes with different cell types such as osteoblasts or their precursor cells, i.e., for example different stem cells, and also with endothelial cells (in mono- and co-cultures) have already been tested and showed impressive results but different limitations exist that does not allow successful transmission of these concepts into the clinical routine [2,6–10].

Strategies for articular cartilage regeneration most often include the addition of different cell types such as chondrocytes or different precursor or stem cells but have also not reached a clinically applicable level [11–13]. Interestingly, it has been shown that blocking of the VEGF pathway supports chondrogenesis [14]. However, also this regeneration concept is also far away from its translation into the clinic.

As a consequence, there is a need for an “optimal” biomaterial applied as basis for successful osteochondral regeneration. Theoretically, this material should provide two components that induce different niches for the simultaneous regeneration of both tissues. One component should provide “bioactive” or inductive properties for establishment of a high scaffold vascularization for bone growth, while the other component should simultaneously induce a reduced vascularization milieu needed for cartilage repair.

In this context, it has been demonstrated that resorbable materials most often induce a tissue reaction cascade called “foreign body response to biomaterials”, which is an inflammatory cellular response whose severity is dependent on the physicochemical properties of a biomaterial [15–20]. This cascade includes different cell types not only involved in material degradation but also contributing to implant bed vascularization by expression of factors such as VEGF [15–20]. Especially macrophages, which have been identified as key components of this tissue reaction cascade, and also biomaterial-associated multinucleated giant cells (BMGCs) have been shown to be potent sources of this angiogenic factor and contribute also in the process of tissue regeneration by expression of anti-inflammatory molecules [15,18,21–23]. Thus, from this point of view, it should be possible to develop more suitable biomaterials for simultaneous bone and cartilage regeneration by modulating the inflammatory tissue response to different parts of such a biomaterial, which includes orchestrating the material-induced vascularization processes based on macrophages and BMGCs, and finally its tissue regenerative abilities.

Additionally, manufacturing methods such as 3D printing have introduced new possibilities for tissue regeneration using scaffolds individually tailored to suit the morphology of tissue defects [24]. The use of 3D printing techniques allows the fabrication of scaffolds in a controllable way with a precise spatial deposition of material components [25]. In this context, polylactic acid (PLA) has been shown to be favorable for scaffold fabrication via 3D printing as the use of this polymer allows for the rapid engineering required in clinical fields like traumatology [25]. Furthermore, it is known that PLA does not induce a high level of bioactivity as tissue responses with a low level of inflammation and also low vascularization rates have been described [26,27]. Thus, a PLA scaffold alone is proposed to be a suitable biomaterial for cartilage repair. In contrast, PLA-based materials most often become combined with other compounds to increase the level of bioactivity and its regenerative potential for bone tissue regeneration [28]. Among the synthetic bone substitute materials based on calcium phosphates (CaP), calcium phosphate-based glasses, in particular the one known as G5 (P_2O_5 - CaO - Na_2O - TiO_2), has been shown to contribute significantly to the vascularization of tissues both *in vitro* and *in vivo* by induction of angiogenesis [29–31]. Thus, it is expected that the angiogenic effect of G5 will support bone tissue regeneration [29,30]. Indeed, the combination of G5 glass with PLA to fabricate a biphasic PLA/G5 scaffold has proven to be a favorable composite bone substitute material based on previous study results by Charles-Harris and colleagues [32]. Furthermore, it has been revealed that the addition of bioglass has also impact on the tissue response to such kind of biphasic scaffold as a higher level of inflammation including BMGCs [33].

Altogether, it should be possible to develop a bi-layered scaffold for promoting both bone and cartilage repair by induction of two different tissue response pattern within one scaffold for guidance of the implant bed vascularization. However, no more profound knowledge of the tissue reactions to those kinds of scaffolds exists until now, this being a pre-requisite for improving their tissue compatibility and regenerative potential.

Accordingly, the aims of the present study are as follows: 1) The development of novel bi-layered scaffolds composed of a polymeric layer (PLA) and a biphasic layer (PLA/G5 glass), 2) the evaluation of the *in vitro* degradation of the scaffolds and 3) the analysis of *in vivo* tissue responses, with special focus on implant bed vascularization and the occurrence of BMGCs, using an established subcutaneous implantation model as well as specialized histological and

histomorphometrical methods allowing the comparison of the type and degree of the tissue response [9,10,16,18–20,22,23,34–38].

2. Materials and methods

2.1. Biomaterial(s)

Poly(95L/5DL)lactic acid (PLA) (Purasorb, PURAC) and polyethylene glycol (PEG) (Mw = 400 Da; Sigma Aldrich) were homogeneously dissolved in chloroform (5%w/v) during 48 h. PEG was added to the PLA matrix as a plasticizer to facilitate scaffold processing [39]. A degradable calcium phosphate glass in the system: $44.5P_2O_5$-$44.5Ca_2O$-$6Na_2O$-$5TiO_2$ (molar %), labeled G5, was used in the form of particles (<40 μm) and added to the polymer blend solution to fabricate biphasic scaffolds [39]. Materials were combined according to the compositions shown in Table 1.

2.1.1. Scaffold fabrication

A nozzle-deposition system (direct-printing tool) (Tissue Engineering 3-Dn-300, Sciperio/nScrypt Inc. Orlando, FL, available in the Rapid Prototyping service of the ICTS "NANBIOSIS", more specifically by the CIBER in Bioengineering, Biomaterials & Nanomedicine (CIBER-BBN)/GBBIT at IBEC, www.ibecbarcelona.eu/biomaterials) was used to fabricate the 3D scaffolds. Briefly, the 3D printing tool combines a nozzle dispensing system and pumping technology with a computer-aided-design/computer-aided-manufacturing (CAD/CAM) approach to build three-dimensional structures of various materials following a procedure previously described [25].

A displaced bi-layer design shown in Fig. 1 was adopted to fabricate the polymeric (PLA), the biphasic (PLA/G5) and bi-layered (composed of a PLA and a PLA/G5 layer) three-dimensional structures described in Fig. 1. For this, polymer and composite blends (Table 1) were dispensed through a G27 (200 μm) nozzle at a pressure ranging between 40 and 80 psi and a motor speed of 7 mm s^{-1}. Polymer and composite inks were kept at 40 ± 5 °C during the printing process by using a heating jacket. Room temperature was maintained at 25 ± 2 °C. Finally, cylindrical scaffolds (4 mm diameter x 4 mm height) were cored from larger 3D printed pieces and used in the degradation studies as well as *in vivo* implantation.

2.2. In vitro degradation study in simulated body fluid (SBF)

In vitro degradation studies were performed by immersing the scaffolds in simulated body fluid (SBF), an acellular solution whose chemical composition is similar to that of blood plasma [40]. Samples were immersed in SBF at 37 °C keeping a volume/mass ratio of 250/1 for 8 weeks, replacing SBF each week. Material dissolution was evaluated in terms of weight loss, molecular weight, morphological variations and mechanical properties in relation to the immersion time. Aging studies were only conducted with PLA and PLA/G5 scaffolds.

Table 1
Composition of the studied materials.

Scaffold	Polymer matrix (w/w %)		G5 particles (w/w%)
	PLA	PEG	
PLA	95	5	–
PLA/G5[a]	95	5	50
Bi-layered[b]	95	5	–
	95	5	50

[a] The percentage shown for the polymer matrix of the PLA/G5 scaffolds corresponds to 50% of the total weight of the scaffold.
[b] Bi-layered scaffolds are a combination of both a PLA and a biphasic PLA/G5 layer as shown in Fig. 1.

2.2.1. Morphological SEM study

Morphological analysis of the 3D structures was carried out by scanning electron microscopy (SEM, JEOL JSM 6400, Tokyo, Japan) to visualize and evaluate the architecture of the 3D scaffolds, surface morphology of the deposited struts, and the distribution and exposure of the glass particles. Cylindrical scaffolds (4 mm diameter x 4 mm height) were cored from larger 3-D printed blocks previously frozen in liquid nitrogen. Moreover, SEM observation was used to visualize any sign of dissolution appearing at the material surface after 8 weeks of immersion in SBF. Additionally, in order to check the exposure of glass particles on the surface of the struts of PLA/G5 scaffolds, an Alizarin Red S assay (ARS) (Millipore, Billerica, MA), which stains calcium red, was performed.

2.2.2. Weight loss

Scaffold weight loss during immersion in SBF was measured by recording the weight changes of the dry specimen after the specified incubation time periods. Different sets of samples were immersed. After 2, 4, 6 and 8 weeks, the scaffolds were removed from the fluid, rinsed in distilled water and dried in an oven for 12 h or until weight stabilization. The percentage of weight loss was computed according to the following equation: wt % = 100 × (Wt −Wo)/Wo, where, Wo is the initial dry weight of the sample and Wt is the dry weight of the sample at time t. Values are expressed as the average of three replicates.

2.2.3. Gel permeation chromatography (GPC) analysis

Weight average molecular weight (Mw) of PLA and PLA/G5 bi-layered scaffolds during degradation was determined by gel permeation chromatography (GPC) using a modular system, composed of an isocratic pump, a vacuum degasser, and refractive index detector (Waters Alliance 2414). Separations were performed in column PSS PFG Analytical 103 Å (Dimensions: 300 × 8.00 mm, particle size: 7 μm). Narrow poly(methyl methacrylate) standards (Fluka) were used for calibration. Samples were analyzed before and after 4 and 8 weeks of immersion in SBF. Analysis was performed at 30 °C, using 50 mM in hexafluoroisopropanol as solvent and filtered (0.22 μm) before injection with a flow-rate of 0.8 ml/min. Acquisition and treatment of chromatographic data was carried out by Empower GPC Software.

2.2.4. Mechanical properties of scaffolds

A Universal Testing Machine (MTS-Bionix 858, MTS Systems Corporation, Eden Prairie, USA) with a 2.5 KN load cell was used to evaluate the mechanical properties of the scaffolds. The samples were tested at a speed of 1 mm/min without preloading. Stress-strain data were computed from load-displacement measurements. The compressive modulus was determined based on the slope of the stress-strain curve in the elastic region. For each material composition, three cubic scaffolds (5 × 5 × 5 mm^3) were tested. Cubic samples were cored from larger 3D printed blocks initially designed in the CAD software. The accurate dimensions of the specimens were measured before the test. Compressive modulus of PLA and PLA/G5 scaffolds was measured before and after 8 weeks of incubation in SBF, in dry condition. A one-way ANOVA test was performed to determine the statistical significance ($p < 0.05$) of the differences in the values of compressive modulus.

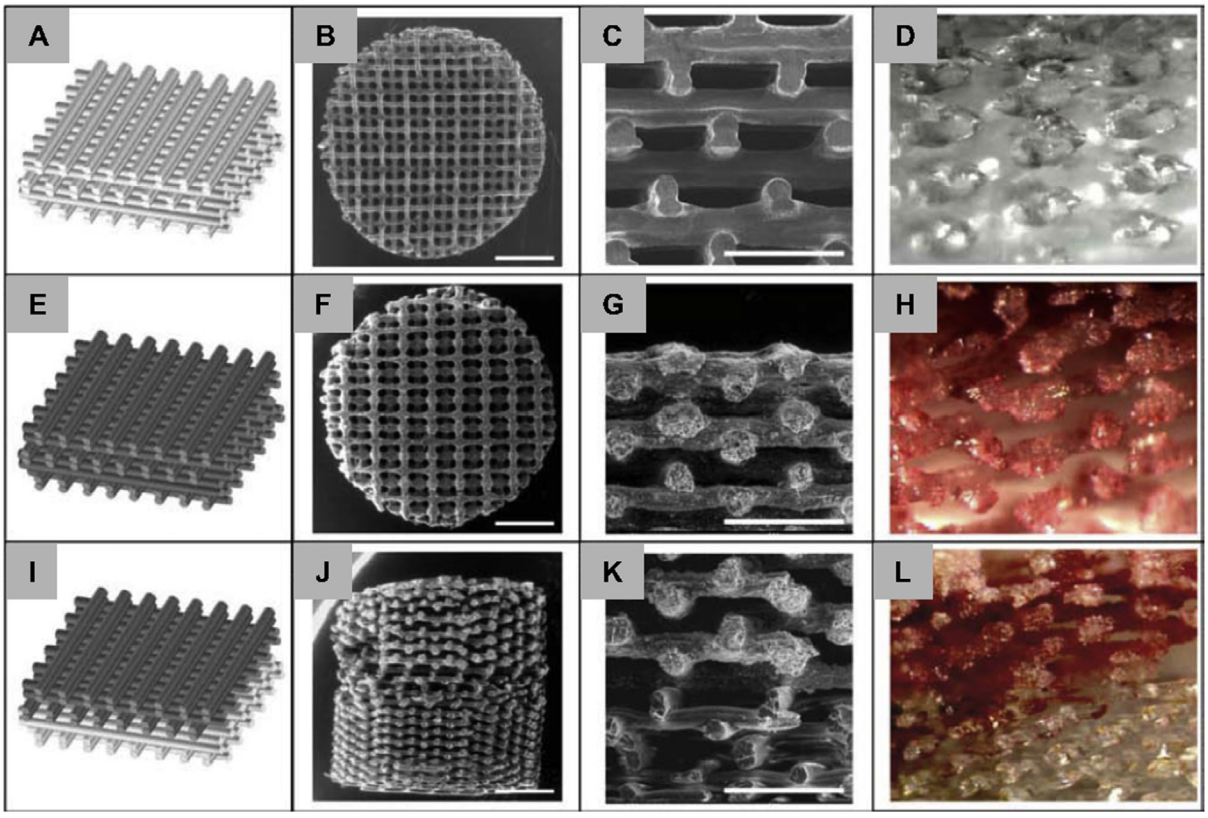

Fig. 1. Structures of the studied scaffolds. (a,e,i) Design of the scaffolds, (b,f,j) axial and (c,g,k) cross sectional SEM micrographs, and (d,h,l) alizarin red staining images of the PLA, PLA/G5 and bi-layered scaffold respectively. (b,f,j: scale bar = 1 mm; d,h,l: scale bar = 500 μm).

2.3. *In vivo* experimental study design and subcutaneous implantation

For these experiments 60 female, 6-8 week-old CD-1 mice (Military Medical Academy, Belgrade, Serbia) were randomly allocated into four study groups. Thus, each of the first three study groups contained 16 animals, which obtained subcutaneous implantation of the three different scaffolds for four study time points, *i.e.* 3, 10, 15 and 30 days, with n = 4 animals per experimental group and time point.

A fourth group ("control") underwent the operation without biomaterial insertion to determine the tissue reaction to the surgical procedure. In total, 12 animals were used in this group for the above-mentioned study time points (n = 3 animals per time point).

The subcutaneous implantation was conducted following the protocol described by Ghanaati and Barbeck et al. [9,10,16,18–20,22,23,34–38]. In brief, the animals were anesthetized via an intraperitoneal injection (10 ml ketamine [50 mg/ml] with 1.6 ml Xylazine [2%]). After shaving and disinfection of the rostral subscapular region, a horizontal incision down to the subcutaneous tissue was made and a subcutaneous pocket was built, in which the biomaterials were inserted. Finally, the wounds were sutured.

The *in vivo* experiments and animal housing were conducted at the Faculty of Medicine (University of Niš, Serbia). The animals were kept under standard conditions (water *ad libitum*, artificial light and regular rat pellet) and standard pre- and postoperative care was ensured. The Local Ethical Committee (Faculty of Medicine, University of Niš, Serbia) authorized the described *in vivo* experiments.

2.3.1. *Explantation procedure and histology*

After the course of the experiments the animals were euthanized with an overdose of the above-described anesthetics and subsequent opening of the thorax. Immediately afterwards, the implanted biomaterials and the surrounding tissue or the area of the control incision were explanted. The histological study was conducted as previously described by Ghanaati and Barbeck et al. [9,10,16,18–20,22,23,34–38]. Thus, the explanted tissue was fixed using a 4% formalin solution for 24 h and afterwards the explants were cut into three segments of identical dimensions including the left margin, the center and the right margin of the biomaterial. Subsequently, dehydration via a series of increasing alcohol concentrations and a final xylol exposure were performed before paraffin embedding. 3–5 μm thick sections were then cut using a rotation microtome (Leica, Wetzlar, Germany) and stained with haematoxylin and eosin (H&E) to choose the best of the three tissue blocks per animal. Following this, five further sections were cut from each tissue block.

After these preparation steps the following stains were used for quantitative and qualitative analyses of the tissue reactions: Hematoxylin and eosin-staining (H&E), azan-staining, Movat pentachrome-staining, tartrate-resistant acid phosphatase (TRAP) staining as well as an immunohistochemical CD31-staining for detection of blood vessels, which included a respective control slide [9,10,16,18–20,22,23,34–38].

2.3.2. *Histological analyses*

The histological analyses to study the outcome of the tissue-biomaterial-interactions within the implantation beds of the scaffolds and their surrounding tissue were conducted using an Eclipse

80i histological microscope (Nikon, Tokyo, Japan) as previously described [9,10,16,18–20,22,23,34–38]. These analyses focused on the evaluation of the following parameters within the framework of the early and the late tissue response related to the implants: fibrosis, hemorrhage, necrosis, vascularization and the presence of neutrophils, lymphocytes, plasma cells, macrophages, (TRAP-positive) biomaterial-associated multinucleated giant cells (BMGCs). Finally, microphotographs were taken with a Nikon DS-Fi1 digital camera and a DS-L2 digital sight control unit (both: Nikon, Tokyo, Japan) connected to the microscope.

2.3.3. Histomorphometrical analyses

The histomorphometrical analyses included the comparative measurements of the vascularization (*i.e.*, vessel density and percent vascularization) as well as the measurement of the extent of BMGCs as described elsewhere [9,10,16,18–20,22,23,34–38]. In brief, so-called "total scans" were generated with the aid of a specialized scanning microscope, which consists of an Eclipse 80i histological microscope combined with a DS-Fi1 digital camera and an automatic scanning table (Prior Scientific, Rockland, MA) connected to an PC system running the NIS-Elements software (Nikon, Tokyo, Japan). The resulting images were composed of 100–120 single images with a 100× magnification in a resolution of 2500 × 1200 pixels and contained the complete biomaterial area as well as the peri-implant tissue. To conduct this study, the azan slides as well as the CD-31 stains were digitized. These images allowed analysis of the tissue reactions to the biomaterials with the use of the NIS-Elements software.

To measure vascularization, the complete area of the biomaterial was first calculated with the "area tool" in the digitized CD-31-stained sections. The vessels were then manually marked also using this tool. For calculation of the vessel density (vessels/mm^2) the number of counted vessels per slide was related to 1 mm of the implant area, while the measurements of the percent vascularization were realized by calculating the percentage of the vascularized implant area based on the summarized vessel areas and the total implant area.

Additionally, for measurement of the extent of the BMGCs, the amounts of these cells were manually counted using the "count tool" of the NIS-Elements software and related to the total implant area (BMGCs/mm^2).

2.3.4. Statistical analyses

Quantitative data are shown as mean ± standard deviation after an analysis of variance (ANOVA), which enabled comparison of the data from the study groups via the GraphPad Prism 6.0c software (GraphPad Software Inc., La Jolla, USA). Statistical differences were designated as significant if p-values were less than 0.05 ($^*p \leq 0.05$), and highly significant if P-values were less than 0.01 ($^{**}p \leq 0.01$) or less than 0.001 ($^{***}p \leq 0.001$).

3. Results

3.1. Scaffold structure

Fig. 1 summarizes the structures of the studied scaffolds, namely PLA, PLA/G5 and the bi-layered scaffolds. As observed by SEM, the 3D printed scaffolds reproduced the predesigned structures very well (Fig. 1a,e,i). Scaffolds with strut diameter of approximately 75 ± 5 μm and pores of 165 ± 5 μm were obtained. In the case of bi-layered scaffolds a clear transition from the polymer (PLA) phase to the biphasic (PLA/G5) phase was observed. Both SEM observation and alizarin red staining (Fig. 1b–d, f-h, j-l) confirmed the presence and exposure of well-distributed glass particles on the surface and inner part of the struts.

3.2. Analysis of scaffold in vitro degradation

The evolution of the physical and chemical properties of the studied scaffolds over an 8-week aging period is shown in Figs. 2 and 3. Fig. 2 displays the surfaces of both PLA and PLA/G5 scaffolds before and after the *in vitro* degradation time. Fig. 2a and b show PLA scaffolds before immersion in SBF, whereas Fig. 2c and d show PLA/G5. In the case of PLA scaffolds, a rather smooth and continuous surface is observed. In the case of the PLA/G5 scaffolds, a rough surface with irregularities and protuberances due to the presence of the glass particles is seen. Fig. 2e,f and 2g-k reveal clearly eroded surfaces after 8 weeks of immersion in SBF. Degradation signs were more visible in the case of PLA/G5 scaffolds than in the case of PLA. PLA/G5 scaffolds exhibited the formation of cracks as well as an increased exposure of the glass particles and a rougher PLA matrix.

Fig. 3a shows the weight variation of PLA and PLA/G5 scaffolds during the aging period. According to the graph, both types of scaffolds underwent an increasing mass loss; however, each material showed a different behavior. PLA/G5 scaffolds displayed an increasing weight loss beginning from the first weeks of immersion in SBF, whereas, in the case of PLA scaffolds, mass loss started after the second week of aging. Weight losses values were significantly different over time and between the two types of scaffolds analyzed with the exception of 4 weeks measurement, where similar values were observed. Though PLA/G5 revealed an initial faster weight loss in comparison to PLA, PLA scaffolds showed a steeper trend, loosing up to 7.98 ± 1.02% of their mass after 8 weeks of degradation.

3.2.1. Evaluation of the molecular weight

The molecular weight (Mw) of the polymer samples was analyzed by GPC; the obtained results are shown in Fig. 3b. A significant reduction of 40.49 ± 0.40% and 42.88 ± 0.86% respectively for PLA and PLA/G5 of the initial average molecular weight was observed for both materials after 4 weeks of study. Moreover, PLA and PLA/G5 scaffolds showed a Mw decrease of 79.34 ± 0.40% and 65.86 ± 0.91% respectively after 8 weeks of immersion in the fluid.

3.2.2. Mechanical test

Fig. 3c displays the variation of the compressive strength of PLA and PLA/G5 scaffolds after 8 weeks of degradation. As expected, there was an initial increase of the compressive strength with the addition of glass particles. In fact, PLA scaffolds showed compressive modulus of around 28.38 ± 3.99 MPa while PLA/G5 showed values around 44.19 ± 2.67 MPa. As observed in the graph, immersion in SBF affected significantly the mechanical stability of the scaffolds. The compressive modulus decreased to 21.17 ± 3.29 MPa in the case of the polymer scaffolds and to 31.08 ± 0.77 MPa for the composites.

3.3. In vivo experiments

3.3.1. Qualitative histological results

The histological analyses revealed that following implantation of the scaffolds no study group gave any signs of necrosis, implant loss or exaggerated inflammatory reactions at any of the study time points (Figs. 4–7).

At day 3 after implantation, a mixture of fibrin and connective tissue fibers combined with a low extent of mononuclear cells were observed within the implantation bed of all scaffolds, *i.e.* both components of the bi-layered scaffolds (Figs. 4b and 5b), the PLA scaffolds (Fig. 6b) as well as the biphasic PLA/G5 scaffolds (Fig. 7b). No signs of ingrowth of complex tissue, vessels orbiomaterial-associated multinucleated giant cells (BMGCs) were observable at

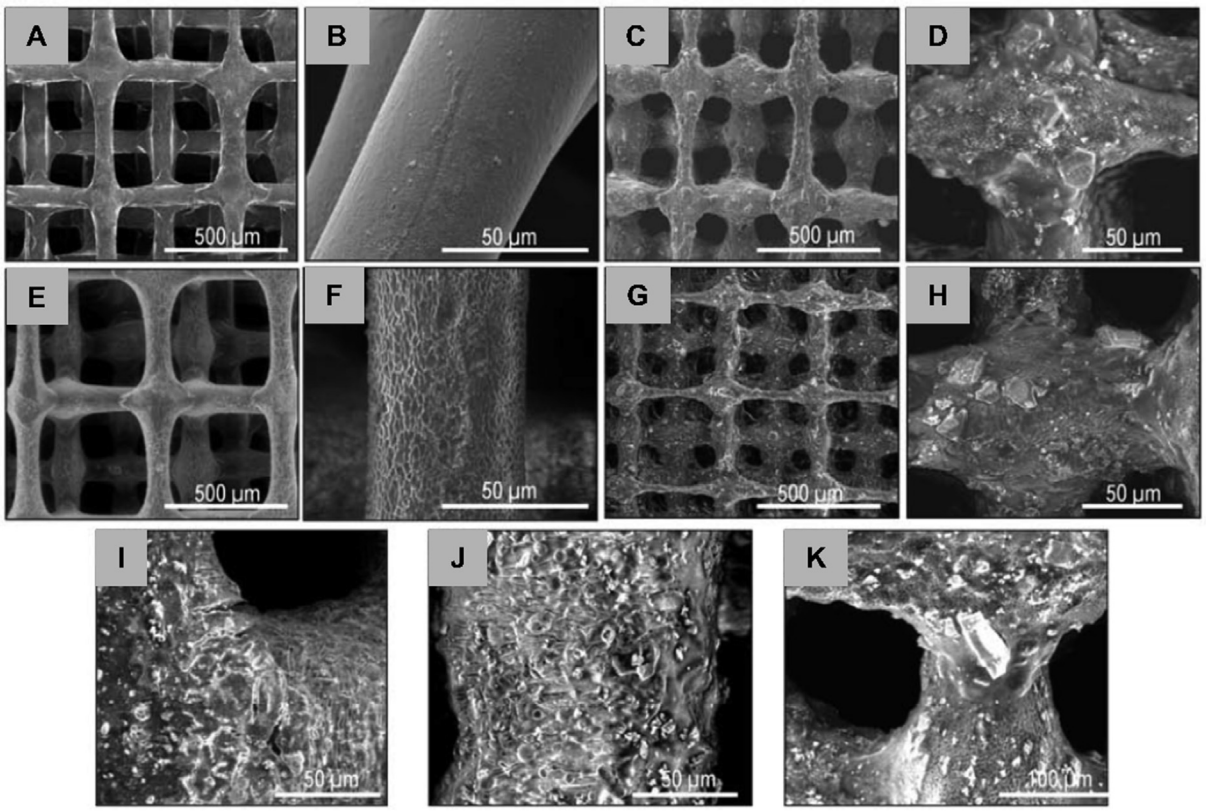

Fig. 2. SEM micrographs indicating surface morphology of PLA and PLA/G5 scaffolds before and after the degradation. In particular: (a,b) PLA and (c,d) PLA/G5 scaffolds before degradation; (e,f) PLA and (g,h) PLA/G5 after degradation. In addition, in (i,j,k) higher magnification images of the PLA/G5 scaffolds after degradation are shown.

this early time point.

Starting at day 10 after implantation, the scaffolds of each study group were integrated within a connective tissue (Figs. 4c, 5c, 6c and 7c). The composition of this tissue was similar at day 15 (Figs. 4d, 5d, 6d and 7d) and day 30 (Figs. 4e, 5e, 6e and 7e). Nonetheless, the composition of the respective peri-implant tissue as well as the presence and the number of material-adherent cells differed between the three different scaffolds.

In the case of the bi-layered scaffolds obvious differences between the tissue reactions to the respective scaffold components, i.e., the PLA components and the biphasic PLA/G5 components, were detected (Figs. 4 and 5). Starting with day 10 the peri-implant tissue of the PLA components of the bi-layered scaffolds showed signs of a low-grade material-induced inflammatory reaction with a fiber-rich connective tissue containing few cells and blood vessels (Fig. 4c). At the surfaces of the PLA component a high number of mononuclear cells were detected, while only few BMGCs were found (Fig. 4c). These tissue reaction patterns did not appear to change at day 15 (Fig. 4d) and day 30 (Fig. 4e). In contrast, the peri-implant tissue of the biphasic PLA/G5 component of the bi-layered scaffolds contained high numbers of cells and blood vessels in combination with a marked infiltration of BMGCs and low numbers of mononuclear cells at their material-tissue-interfaces (Fig. 5c–e).

Histology revealed that both control materials, *i.e.* the mono-layered PLA and biphasic PLA/G5 scaffolds, induced tissue reactions comparable to those elicited by the components of the bi-layered scaffolds (Figs. 6 and 7). Thus, the PLA scaffolds were found embedded within a fiber-rich connective tissue starting at day 10 up to day 30, and induced low numbers of material-adherent MNGCs combined with high amounts of mononuclear cells and low vascularization (Fig. 6c–e). In contrast, the mono-layered PLA/G5 scaffolds were found embedded within a cell and vessel-rich connective tissue up to day 30 after implantation (Fig. 7c–e). This material induced high numbers of adherent BMGCs, while mononuclear cells were only involved to a minor extent in the tissue reaction (Fig. 7c–e).

Additionally, the histological analysis of TRAP expression also showed that the amount of TRAP-positive BMGCs within the peri-implant tissue of the PLA component of the bi-layered scaffolds was low at all study time points (Fig. 8a) and comparable to the number within the group of the mono-layered PLA scaffolds (Fig. 8b). Furthermore, the histological observations showed that higher numbers of TRAP-positive BMGCs were found within the implant bed of the biphasic PLA/G5 component of the bi-layered scaffolds (Fig. 8c). Comparable numbers of these cells were also found within the peri-implant tissue of the mono-layered PLA/G5 scaffolds (Fig. 8d).

3.3.2. Quantitative histomorphometrical results

3.3.2.1. Results of the vessel density measurements. The comparative measurements of the vessel density showed that none of the implantation beds of the three scaffold types showed any signs of vessel ingrowth at day 3 after implantation (Fig. 9a). In contrast, the control group showed a moderate amount of vessel ingrowth (7.94 ± 1.97 vessels/mm^2) significantly higher than the three study groups (PLA, PLA/G5 and bi-layered scaffolds) ($^{**}p \leq 0.01$) (Fig. 9a).

At day 10 after implantation, the analyses revealed that significantly higher number of vessels ($^{**}p \leq 0.01$) were found within the implantation beds of the PLA/G5 component of the bi-layered scaffolds (18.99 ± 2.67 vessels/mm^2) and of the mono-layered PLA/G5 group (20.44 ± 3.47 vessels/mm^2) in comparison to the number of vessels found within the implantation beds of the PLA

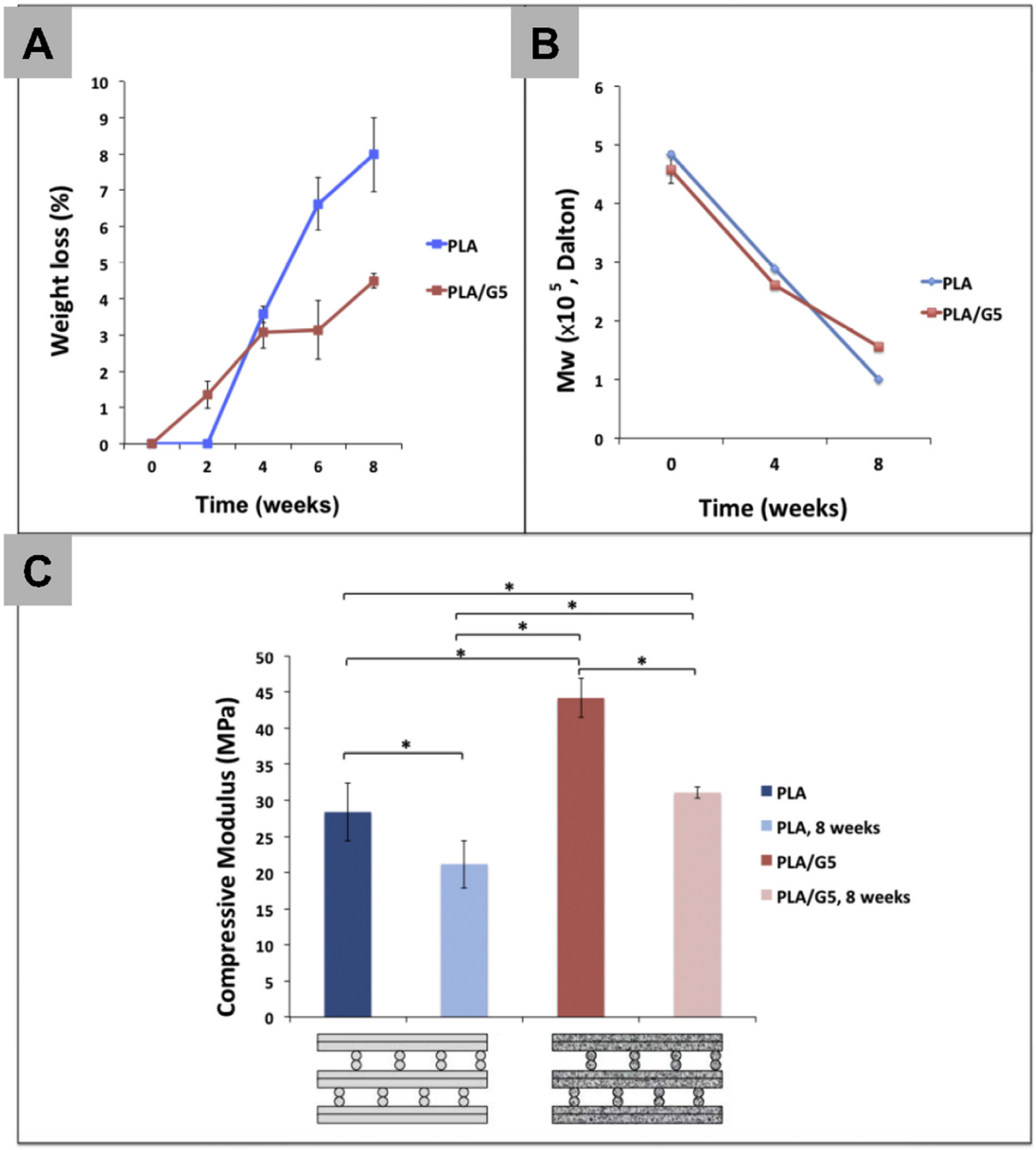

Fig. 3. (a) Weight loss, (b) molecular weight evolution, and (c) mechanical test of PLA and PLA/G5 scaffolds over an 8-weeks aging period (*p ≤ 0.05).

component (7.94 ± 1.97 vessels/mm^2), the mono-layered PLA scaffolds (7.74 ± 3.71 vessels/mm^2), and the control group (9.13 ± 0.98 vessels/mm^2) (Fig. 9a). Interestingly, no significant differences were found between the vessel density values of the biphasic PLA/G5 component and the mono-layered PLA/G5 implants (Fig. 9a). Additionally, no differences were observed between the PLA component of the bi-layered scaffolds, the mono-layered PLA scaffolds and the control group (Fig. 9a). Thereby, the total number of vessels detected within the whole implantation beds of the bi-layered scaffolds (14.25 ± 3.61 vessels/mm^2) was between the values of all other study groups without any significant differences being detected (Fig. 9a).

At day 15 after implantation significantly higher vessel numbers were still found within the implant beds of the biphasic PLA/G5 component of the bi-layered scaffolds (36.39 ± 7.13 vessels/mm^2) and within that of the mono-layered PLA/G5 scaffolds (33.59 ± 5.27 vessels/mm^2) compared to that of the PLA component (14.98 ± 4.28 vessels/mm^2), the mono-layered PLA scaffolds (12.84 ± 6.05 vessels/mm^2) and the control group (9.95 ± 1.69 vessels/mm^2) (**p ≤ 0.01) (Fig. 9a). Thus, no significant differences were found; either between both PLA/G5 scaffolds or between both PLA scaffolds and the control group (Fig. 9a). Additionally, the vessel numbers of the whole bi-layered scaffolds were significantly higher only compared to the values of the control group (**p ≤ 0.01) (Fig. 9a). The histomorphometrical analysis showed that the numbers of vessels again were significantly higher in the group of

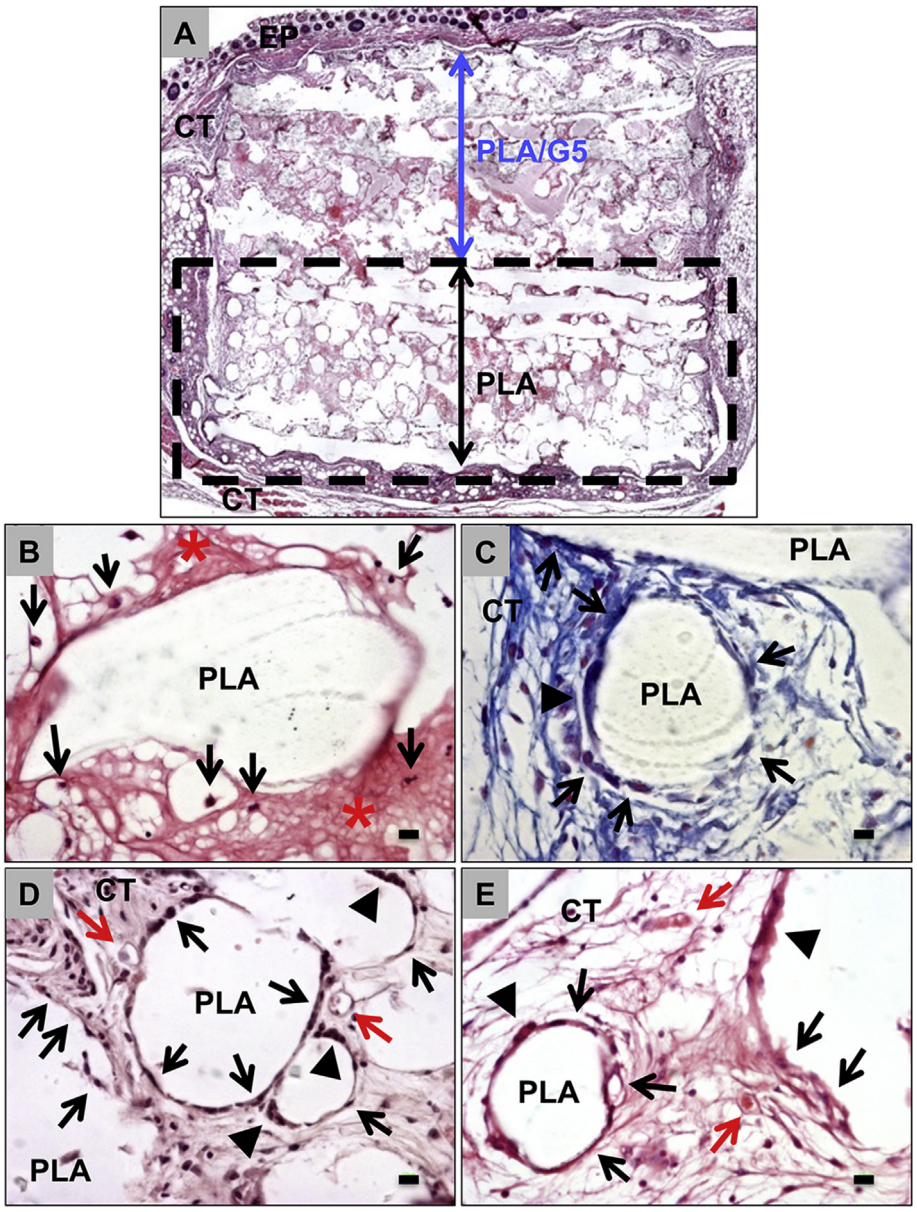

Fig. 4. Tissue reaction to the PLA component of the bi-layered scaffolds within the subcutaneous connective tissue (CT). (a) Representative overview of an implantation bed of a bi-layered scaffold at day 10 after implantation. Biphasic PLA/G5 layer = blue double arrow, PLA layer = green double arrow and dashed line ("total scan", HE-staining, 100× magnification). (b–e) Tissue reactions to the PLA component of the bi-layered scaffolds at day 3 (b), day 10 (c), day 15 (d) and day 30 (e) after implantation. Mixture of collagen fibers and fibrin = red asterisks, mononuclear cells = black arrows, vessels = red arrows, multinucleated giant cells = arrowheads (b, d and e: HE-staining, c: Azan-staining, 400× magnifications, scale bars = 10 μm).

the PLA/G5 components of the bi-layered scaffolds (35.94 ± 6.51 vessels/mm^2) and that of the mono-layered PLA/G5 scaffolds (32.82 ± 5.39 vessels/mm^2) compared to that in all other study groups at day 30 after implantation (**$p \leq 0.01$) (Fig. 9a). Nevertheless, no significant differences were found between the values of these study groups (Fig. 9a). Furthermore, the vessel numbers in the groups of the PLA components (14.03 ± 5.99 vessels/mm^2) and mono-layered PLA scaffolds (13.65 ± 2.79 vessels/mm^2) as well as of the control group (10.03 ± 0.91 vessels/mm^2) were comparable (Fig. 9a). The values of the total implant area of the bi-layered scaffolds (19.74 ± 4.78 vessels/mm^2) at day 30 after implantation were only significantly higher than the values of the control group (*$p \leq 0.05$) (Fig. 9a).

3.3.2.2. Results of percentage vascularization. The histomorphometrical analyses showed that at day 3 after implantation only the control group displayed vascularization (0.06 ± 0.01%), showing significantly higher percentages than the other three study groups (**$p \leq 0.01$), whose implantation beds did not show any vascularization (Fig. 9b).

At day 10 after implantation both the PLA/G5 component of the bi-layered scaffolds (1.26 ± 0.29%) and the mono-layered PLA/G5 scaffolds (1.32 ± 0.15%) showed the highest vascularization values without significant differences between them (Fig. 9b). Furthermore, the values of these two groups were significantly higher compared to that of the PLA component of the bi-layered scaffolds (0.68 ± 0.27%) and of the mono-layered PLA scaffolds (0.52 ± 0.19%) (**$p \leq 0.01$) and also compared to the values of the total bi-layered

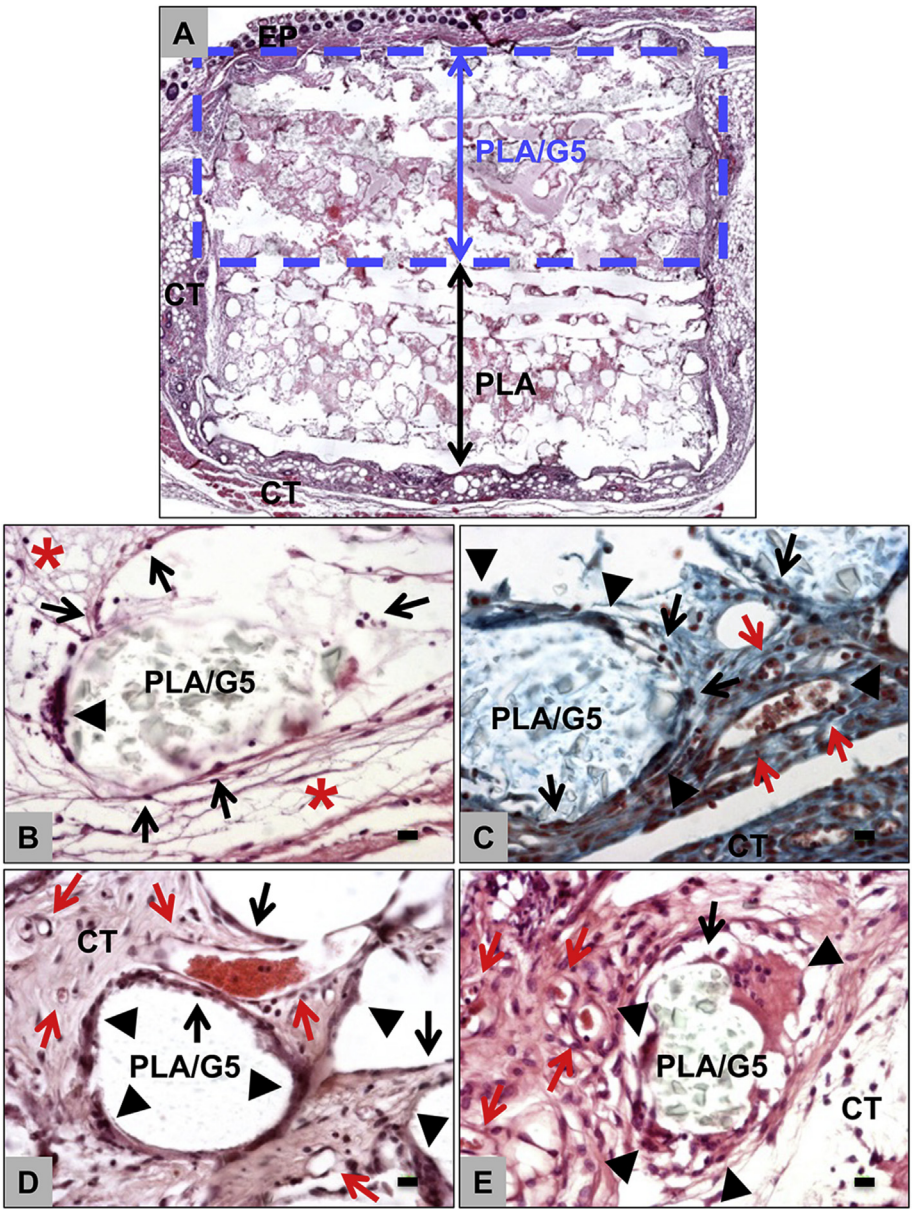

Fig. 5. Tissue reaction to the PLA/G5 component of the bi-layered scaffolds within the subcutaneous connective tissue (CT). (a) Representative overview of an implantation bed of a bi-layered scaffold at day 10 after implantation. Biphasic PLA/G5 layer = blue double arrow and dashed line, PLA layer = green double arrow ("total scan", HE-staining, 100× magnification). (b–e) Tissue reactions to the biphasic PLA/G5 layer at day 3 (b), day 10 (c), day 15 (d) and day 30 (e) after implantation. Network of collagen fibers and fibrin = red asterisks, mononuclear cells = black arrows, multinucleated giant cells = arrowheads, vessels = red arrows (b, d and e: HE-staining, c: Azan-staining, 400× magnifications, scale bars = 10 μm).

scaffolds (0.85 ± 0.15%, $^{*}p \leq 0.05$) and of the control group (0.08 ± 0.02%, $^{***}p \leq 0.001$) (Fig. 9b). The values of the PLA component and of the mono-layered PLA scaffolds as well as of the total bi-layered scaffolds were also significantly higher compared to that of the control group ($^{*}p \leq 0.05/^{**}p \leq 0.01$) (Fig. 9b).

At day 15 after implantation, the vascularization percentage of both the PLA/G5 component of the bi-layered scaffolds (1.68 ± 0.39%) and the mono-layered PLA/G5 group (1.81 ± 0.23%) was still the highest ($^{**}p \leq 0.01/^{***}p \leq 0.001$) (Fig. 9b). The PLA component of the bi-layered scaffolds (0.91 ± 0.37%), the mono-layered PLA scaffolds (0.81 ± 0.15%) and the total bi-layered scaffolds (1.68 ± 0.39%) still showed similar values (Fig. 9b). Moreover, all study groups revealed significantly higher values than the control group (0.29 ± 0.06%, $^{*}p \leq 0.05/^{**}p \leq 0.01/^{***}p \leq 0.001$) (Fig. 9b).

At day 30, it was revealed that scaffolds containing G5 induced higher vascularization percentages (PLA/G5 phase of bi-layered scaffolds: 1.79 ± 0.34% and PLA/G5 scaffolds: 1.59 ± 0.28%) than the rest of the study groups ($^{**}p \leq 0.01/^{***}p \leq 0.001$) (Fig. 9b). Still no differences were found between the values obtained for the PLA component of the bi-layered scaffolds (0.88 ± 0.39%) and the mono-layered PLA scaffolds (0.72 ± 0.24%), whose values were also similar to that of the total bi-layered scaffolds, but significantly higher compared to the control group (0.29 ± 0.06%, $^{*}p \leq 0.05$) (Fig. 9b). Additionally, the values of the bi-layered scaffolds were also significantly higher than those of the control group ($^{**}p \leq 0.01$) (Fig. 9b).

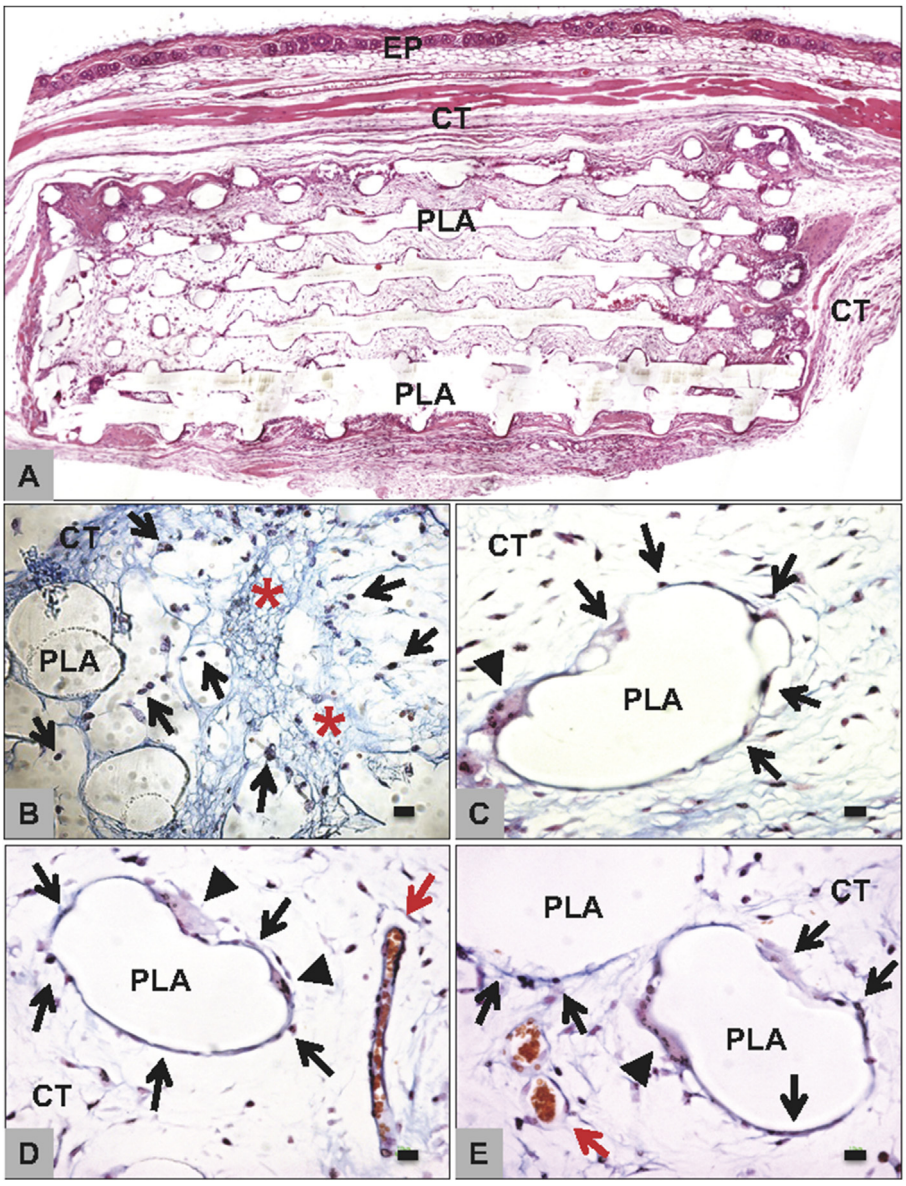

Fig. 6. Tissue reaction to the mono-layered PLA scaffolds within the subcutaneous connective tissue (CT). (a) Representative overview to an implantation bed of a mono-layered PLA scaffold at day 10 after implantation ("total scan", HE-staining, 100× magnification). (b–e) Tissue reactions to the PLA scaffold at day 3 (b), day 10 (c), day 15 (d) and day 30 (e) after implantation. Network of collagen fibers and fibrin = red asterisks, mononuclear cells = black arrows, multinucleated giant cells = black arrowheads, vessels = red arrows (b–e: Azan-staining, 400× magnification, scale bar = 10 μm).

3.3.2.3. Results of the biomaterial-associated multinucleated giant cell (BMGC) measurements. The histomorphometrical analysis of the extent of biomaterial-associated multinucleated giant cells (BMGCs) showed that the implantation beds of all study groups did not contain cells of this lineage at day 3 after implantation (Fig. 9c).

At day 10 after implantation the analyses revealed that within the implantation beds of the PLA/G5 component of the bi-layered scaffolds (51.13 ± 8.26 BMGCs/mm^2) and the mono-layered PLA/G5 scaffolds (46.57 ± 7.02 BMGCs/mm^2) significantly higher numbers of BMGCs were found in comparison to all other study groups (*p ≤ 0.05/**p ≤ 0.01) (Fig. 9c). Furthermore, significantly higher numbers of BMGCs were found for the total bi-layered scaffolds (32.54 ± 5.46 BMGCs/mm^2) compared to the values in the other groups, namely the group of the PLA components of the bi-layered scaffolds (23.91 ± 6.13 BMGCs/mm^2) and of the mono-layered PLA scaffolds (21.03 ± 4.25 BMGCs/mm^2) (*p ≤ 0.05) (Fig. 9c). Thus, no differences were found comparing the values of the latter two groups (Fig. 9c).

At day 15 no significant differences in the number of BMGCs were observed between the group of PLA/G5 component of the bi-layered scaffolds (49.29 ± 9.17 BMGCs/mm^2) and that of the mono-layered PLA/G5 scaffolds (44.61 ± 8.96 BMGCs/mm^2), while their values differed significantly in comparison to the rest of the groups (**p ≤ 0.01) (Fig. 9c). Additionally, no differences were found between group of the PLA component of the bi-layered scaffolds (22.08 ± 5.83 BMGCs/mm^2), the group of the mono-layered PLA scaffolds (21.03 ± 4.25 BMGCs/mm^2) and the complete bi-layered study group (31.68 ± 5.96 BMGCs/mm^2) (Fig. 9c).

Also, at day 30 after implantation a substantially higher number of BMGCs was found in the groups containing the PLA/G5 phase (PLA/G5 bi-layered: 53.19 ± 8.60 BMGCs/mm^2 and PLA/G5 scaffolds: 56.41 ± 7.95 BMGCs/mm^2), these values being significantly

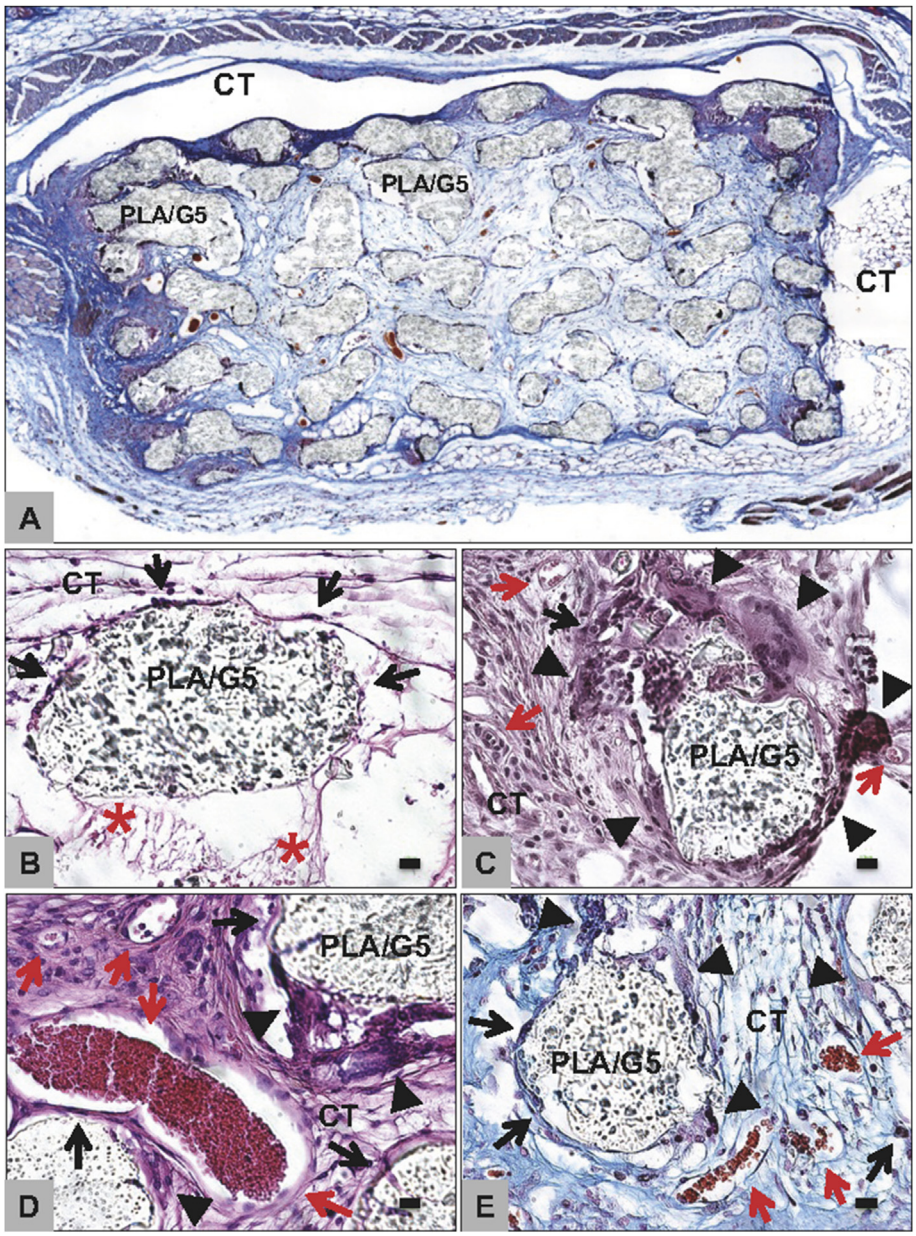

Fig. 7. Tissue reaction to the mono-layered PLA/G5 scaffolds within the subcutaneous connective tissue (CT). (a) Representative overview to an implantation bed of a mono-layered PLA/G5 scaffold at day 10 after implantation. ("total scan", Azan-staining, 100× magnification). (b–e) Tissue reactions to the PLA/G5 scaffold at day 3 (b), day 10 (c), day 15 (d) and day 30 (e) after implantation. Mixture of collagen fibers and fibrin = red asterisks, mononuclear cells = black arrows, multinucleated giant cells = black arrowheads, vessels = red arrows (b–d: HE-staining, e: Azan-staining, 400× magnification, scale bar = 10 μm).

higher than the ones obtained for the other groups (**$p \leq 0.01$) (Fig. 9c). At this latest study time point the numbers of BMGCs in the implantation beds of the PLA component of the bi-layered scaffolds (24.22 ± 4.21 BMGCs/mm^2), the group of the mono-layered PLA scaffolds (26.52 ± 5.11 BMGCs/mm^2) and the study group of the total bi-layered scaffolds (42.41 ± 10.85 BMGCs/mm^2) still did not differ significantly (**$p \leq 0.01$) (Fig. 9c).

4. Discussion

This study aimed to explore a novel therapeutic approach to promote both bone and cartilage tissue regeneration by modulating the inflammatory tissue response on basis of the fabrication of bi-layered 3-D printed scaffolds. In this context, the different chemical composition of the scaffold components should induce different vascularization pattern of their respective implant beds based on the different induction of both macrophages and biomaterial-associated multinucleated giant cells (BMGCs), which have been shown to be potent sources of the vascular endothelial growth factor (VEGF) [16].

The bi-layered scaffolds based on PLA and PLA combined with CaP based bioactive glass G5 were developed by 3-D printing allowing the fabrication of 3-D structures with precise and reproducible geometry. Such an approach has been shown to permit more accurate conclusions than those obtained from random architectures with high variability among the samples [41]. The addition to the PLA scaffolds of the G5 glass, which has been demonstrated to contribute significantly to the vascularization of

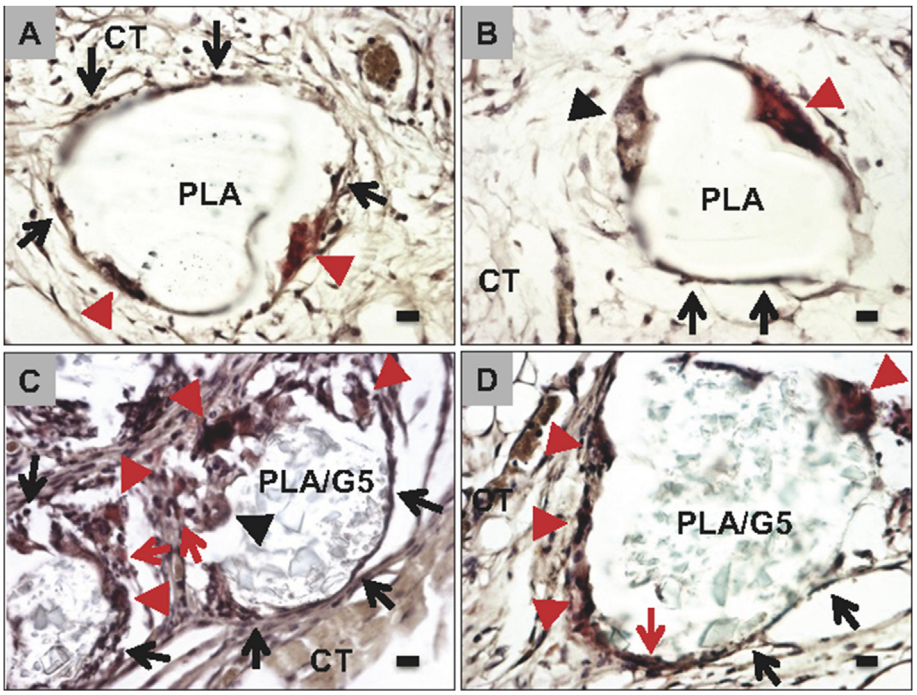

Fig. 8. Representative images of the TRAP activity of material-adherent mono- (arrows) and multinucleated (arrowheads) cells at day 15 after implantation within the subcutaneous connective tissue (CT). PLA component of the bi-layered scaffolds (a) and of the mono-layered PLA scaffolds (b), PLA/G5 component of the bi-layered scaffolds (c) and of the mono-layered PLA/G5 scaffolds (d). TRAP-positive multinucleated giant cells = red arrowheads, TRAP-positive mononuclear cells = red arrows, TRAP-negative multinucleated cells = black arrowheads, TRAP-negative mononuclear cells = black arrows (all images: TRAP-staining, 400× magnification, scale bar = 10 μm).

tissues both *in vitro* and *in vivo* by induction of angiogenesis, was expected to support bone tissue regeneration based on a previous *in vitro* study [29,30]. In this work, the fabrication methods and different *in vitro* analysis methods including measurements of weight loss, molecular weight, morphological variations and mechanical properties were used to study the scaffold properties before and after the *in vitro* degradation period. Furthermore, the *in vivo* tissue response was analyzed using an established subcutaneous implantation model as well as previously described histological and histomorphometrical methods [9,10,16,18–20,22,23,34–38].

The *in vitro* degradation study conducted up to 8 weeks initially showed that both the PLA and the PLA/G5 scaffolds maintained their structural integrity without completely losing the original architecture and strength. However, an increase of surface roughness was observed for both types of samples. In the case of the PLA scaffolds, the increase of roughness was mostly attributed to an enlargement of the micro- and nanopores already present at the surface of the strut due to the fabrication process [25]. In the case of the PLA/G5 scaffolds, higher surface erosion was noticed. The struts containing G5 glass particles were slightly thinner than before degradation and showed superficial cracks. This phenomenon could be attributed to an easier penetration of fluid at the interface between the PLA matrix and the hydrophilic G5 particles, thus leading to an acceleration of the hydrolytic degradation of the polymer matrix, and the formation of cracks at the strut surface [42]. As a consequence, glass particles were more exposed at the surface.

Furthermore, weight loss studies showed significant differences between both types of scaffolds. PLA/G5 exhibited a higher and progressive weight loss during the first two weeks of *in vitro* degradation. However, between weeks 4 and 6 its degradation rate decreased significantly. Finally, after 8 weeks, the composite scaffold showed a weight loss of about 4.5%. In contrast, PLA scaffold weight loss started only after two weeks of immersion, overtaking the PLA/G5 at 4 weeks and reaching the 8% of weight loss after 8 weeks. As mentioned before, the weak interface between the polymeric PLA and glass particles could be the driving agent of the faster weight loss or degradation in PLA/G5 scaffolds in the initial weeks. From the fourth week until the end of the immersion period, weight loss evolution was influenced by two other events strictly related to the incorporation of G5 particles. The first one consisted in the possible formation of CaP precipitates on the surface of the biphasic PLA/G5 scaffolds as observed by Navarro et al. in a previous study on similar materials [42]. To explain the second event, it is important to remark that PLA generates acidic products (mostly lactic acid) that can decrease the pH of the surrounding solution, thus accelerating the degradation in an autocatalytic way [43]. Hence, in the case of the biphasic PLA/G5 scaffolds, G5 degradation by-products acted as a buffer agent for the surrounding solution, mitigating the degradation process. Both phenomena acted synergistically to slow down the composite scaffold weight loss, which became lower than the polymeric one after 8 weeks. Nevertheless, it is interesting to observe that, excluding the brief accelerated loss of the biphasic material at early time points, weight loss curves for the 3D scaffolds were quite similar to the ones previously reported for 2D PLA/G5 films [39]. Final weight loss percentages were between 4.5 and 8% for both materials in 2D and 3D. The presence of PEG domains strongly influenced the degradation rate of the materials [39] The effect of hydrophilic PEG, enhancing the fluid erosion at the interface between polymer and G5 particles, led to a faster degradation of the PLA/G5 scaffolds during the first weeks of immersion. Furthermore, PEG showed a more determinant effect in the degradation process of the PLA scaffolds leading to higher weight loss after 8 weeks.

To confirm the dissolution of the scaffolds, gel permeation chromatography (GPC) analysis was carried out. A continuous decrease in molecular weight values was observed due to the

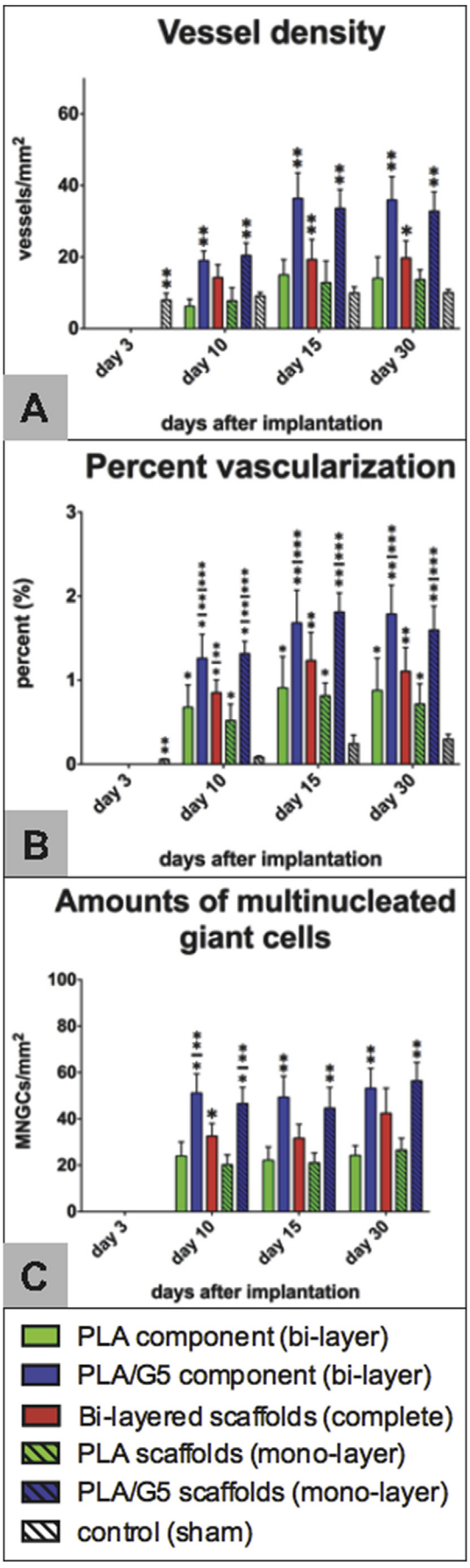

progressive cleavage of the polymeric chains. In particular, it seems that the PLA/G5 reduction of molecular weight was less than for PLA alone. These results were in good agreement with the weight loss analysis previously described [39]. It could be attributed to the already mentioned effect of PEG in the PLA/PEG blend and the higher amount of PEG in the PLA scaffold in comparison to the PLA/G5 scaffolds, where 50% (w/w) is composed by glass particles.

It is known that an ideal scaffold for bone regeneration should gradually transfer the load to the newly forming bone during degradation [41,44]. Thus, a suitable choice of material and scaffold design should be made in order to tune both degradation rate and mechanical properties. The evaluation of the mechanical properties of the scaffolds showed that the values of compressive modulus were diminished for both scaffolds after 8 weeks of immersion in SBF. Thus, the biphasic PLA/G5 scaffold became weaker than the PLA ones. As previously mentioned, the surface of the PLA/G5 scaffolds seemed to be mainly subjected to liquid erosion because of the fluid penetration at the interface between polymer and glass particles. Hence, it is presumed that the formation of fractures together with the weakening of polymer-glass adhesion led to the reduction of its mechanical properties. Nevertheless, even after the studied degradation process, the biphasic scaffolds presented higher modulus than that shown by the polymeric scaffold before degradation.

The results of the *in vivo* analyses showed that the two components of the bi-layered scaffolds, *i.e.*, the monophasic PLA- and the biphasic PLA/G5-components induced inflammatory tissue reactions with different severities. The tissue reaction to the PLA component included a low number of BMGCs and minimal vascularization of its implant beds, which suggest a mild severity of a material-related foreign body response. In contrast, the addition of G5 particles (PLA/G5) induced a tissue reaction involving a significantly higher number of BMGCs and also a significantly higher implant bed vascularization. These results confirm previous study results that demonstrated the pro-angiogenic potential of G5 both *in vitro* and *in vivo* [29,30]. Interestingly, the present results show that the higher implant bed vascularization is accompanied with the higher induction of BMGCs. Also, further study results have been shown that the induction of BMGCs in many cases correlates with increased implant bed vascularization [16,18–20,22,23,34–38].

Two different molecular pathways for induction of the observed increase of vascularization are conceivable, which are at least coupled and described as “foreign body response to biomaterials” [15]. On the one hand, it has been demonstrated that this material-associated multinucleated cell type is also a strong source of VEGF and also of the heme oxygenase 1 (HO-1), which are known to be strong promoters of the process of angiogenesis [23]. Additionally, their production is also well known in mononuclear cells of the monocyte and macrophage lines [15,21,22]. Thus, the material-induced inflammatory tissue response including the permanent transport to and from of different cell types to the implantation bed is a factor for the increase of vascularization as this transport mechanisms become processed via the blood way.

On the other hand, it has been suggested that the higher implant bed vascularization might be based on the Ca^{2+} release, which has been shown to activate endothelial progenitor cells and elicit a subsequent release of vascular endothelial growth factor (VEGF) by activation of the calcium-sensing receptor (CaSR), and a subsequent intracellular cascade that finally leads to increased angiogenesis

Fig. 9. Histomorphometrical results of (a) the vessel density, (b) the percent vascularization and (c) the amounts of multinucleated giant cells (*$p \leq 0.05$, **$p \leq 0.01$, ***$p \leq 0.001$).

[29,45].

In this context, especially BMGCs have been shown to be involved in the degradation of biomaterials via phagocytosis [15,23,34,46,47]. In this context, McNally and colleagues have been revealed this multinucleated cell type exhibits features of phagocytosis with participation of the endoplasmic reticulum [47]. Moreover, it has been shown by Barbeck et al. that a subcellular compartment was detectable between the biomaterial surfaces and the material-adherent poles of the giant cells, although further results have been shown that this cell type can be assigned to the "lineage" of the foreign body giant cells [34]. This "extracellular" structure is similar to the clear zone of osteoclasts, in which an acid microenvironment becomes established to degrade the different components of the bone matrix [48]. Thus, this subcellular compartment seems to be an extracellular equivalent to phago- or lysosomes for processing cell-driven biomaterial dissolution and fragmentation for further phagocytosis. Furthermore, material fragments of a phycogenic bone substitute have shown to be detectable within intracellular vacuoles, which also contained the tartrate-resistant acid phosphatase (TRAP) enzyme [46]. Even this metalloenzyme has been shown to be involved in the process of the degradation of different various phosphate esters and anhydrides under acidic reaction conditions such as the analyzed PLA/G5 scaffolds that show a significant higher induction of TRAP-positive BMGCs [49]. Based on this data, it is assumable that the BMGCs liberate calcium from the analyzed material and after phagocytosis and transcytosis the Ca^{2+} ions become released into the surrounding tissue comparable to the bone resorption process processed by osteoclasts [48]. Thus, the degradation process mediated by BMGCs and the Ca^{2+} release might induce a further increase of angiogenesis and implant bed vascularization as a result of the material-induced inflammatory tissue reaction. Altogether, the processes of angiogenesis and bone growth are coupled with inflammation and degradation process of a biomaterial as previously described [22,23].

However, the question remains why the PLA/G5 scaffolds induce a higher number of BMGCs combined with an increased TRAP expression. In this context, it has been shown that the occurrence of TRAP-positive and presumably pro-inflammatory cells such as macrophages and BMGCs in the implant beds of different biomaterials are dependent on the physicochemical material characteristics [15,16,19,20,22,23,34–38]. Moreover, it is known that giant cell formation is dependent on biomaterial surface properties that initially induce a material-specific adsorption of (a spectrum of) proteins [15]. Hence, it is presumable that the higher number of TRAP-positive BMGCs is related to the surface characteristics of the bioactive G5 glass in contrast to the mono-layered PLA scaffolds. The latter appear to induce an accumulation of proteins such as the fibrinogen molecule and a subsequent folding of these proteins that subsequently trigger the inflammatory tissue reaction [15]. For example, it is known that the exposure of "pro-inflammatory" amino acid sequences such as the Mac-1-binding site within the D domain of the fibrinogen molecule could function as cellular binding site for monocytes or neutrophils, which triggers inflammatory cellular responses [50–52]. Interestingly, the initial analysis of the *in vitro* degradation demonstrated that the PLA components or scaffolds exhibit smooth surfaces, while the biphasic ones were shown to be rather rough. In this context, other smooth biomaterial surfaces have been shown to elicit a foreign body reaction involving mononuclear cells such as macrophages, rather than multinucleated giant cells [15,53,54]. Thus, it could be presumed that this material factor has determined the observed tissue reactions in case of the PLA scaffolds, while the rougher surface topography of the PLA/G5 scaffolds induced the tissue reaction involving significantly higher numbers of BMGCs.

Altogether, the presented results lead to the conclusion that the G5 glass has indirect influence on the molecular induction of implant bed vascularization. In this process, the inflammatory tissue reaction and especially BMGCs are "interposed" mediating the release of biologically effective ions such as Ca^{2+} ions. Thus, it might be possible to take advantage of the inflammatory reactions to a biomaterial for the process of tissue reaction. In case of the analyzed bi-layered scaffolds it seems to be feasible to use even the different tissue reactions to the both layers, i.e., the PLA and the PLA/G5 layer, for guiding the implant bed vascularization to allow better healing of osteochondral defects.

Additionally, the data from both the histological observations and the histomorphometrical measurements revealed that the tissue responses to the distinct layers of the bi-layered scaffolds were localized to their respective implantation areas in spite of their direct proximity. Furthermore, these results were substantiated by comparison with the "second" control materials, *i.e.* the mono-layered PLA and PLA/G5 scaffolds, which show comparable tissue reactions. Furthermore, this data show that it is possible to implant and study the material-related tissue reaction to more than one biomaterial with a minimum separation between them, in the same experimental animal as the inflammatory tissue reactions to a biomaterial seems to be restricted to some micrometers. This could contribute to a significant reduction in the numbers of animals required, which is in accordance with the principle of the **3R**s (**R**eplacement, **R**eduction and **R**efinement) [55]. These data raise the question of the possible application of high-throughput multi-screening devices for the analyses of multiple biomaterials in one animal.

5. Conclusion

In this study, a novel approach to heal bone and cartilage defects with a bi-layered material based on different tissue responses and different vascularization pattern has been explored. Therefore, a scaffold composed of two different layers, PLA and biphasic PLA/G5, has initially been fabricated and systematically characterized. An *in vitro* degradation analysis showed that scaffolds kept their structural integrity, while changes in morphology were observed, especially for the PLA/G5 scaffold. Weight loss was higher for the PLA scaffold, confirming the important effect of PEG in the degradation process. Mechanical properties decreased with progressive degradation. Nevertheless, the PLA/G5 scaffolds presented higher compressive modulus than PLA scaffolds, confirming the reinforcing effect of G5 even after immersion time. Finally, *in vivo* evaluation of the tissue reactions showed prevalence of mononucleated cells in the implant beds of the PLA scaffolds that did not undergo relevant vascularization. In contrast, the addition of the bioactive G5 glass induced an elevated number of biomaterial-associated multinucleated giant cells and a significantly higher implant bed vascularization. Based on these results, this bi-layered scaffold may be a potential material for the healing of tissue defects of bone and cartilage tissue. Additionally, these results beg the question for reduction of the number of experimental animals required for preclinical biomaterial testing with special view on the principle of the **3R**s (**R**eplacement, **R**eduction and **R**efinement) as the different tissue responses to the distinct layers of the bi-layered scaffolds were localized to their respective implantation areas in spite of their direct proximity. Based on this knowledge, more than one biomaterial could simultaneously be analyzed into one experimental animal as no interference between the respective implants beds may exist.

Acknowledgements

We thank the Spanish MINECO for supporting the project MAT2012-38793 and for funding MN through the Ramón y Cajal program and TS through the "Personal Técnico de Apoyo" subprogram.

References

[1] D.J. Huey, J.C. Hu, K.A. Athanasiou, Unlike bone, cartilage regeneration remains elusive, Science 338 (6109) (2012 Nov 16) 917–921.
[2] A.R. Amini, C.T. Laurencin, S.P. Nukavarapu, Bone tissue engineering: recent advances and challenges, Crit. Rev. Biomed. Eng. 40 (5) (2012) 363–408.
[3] J. Street, M. Bao, L. deGuzman, S. Bunting, F.V. Peale Jr., N. Ferrara, H. Steinmetz, J. Hoeffel, J.L. Cleland, A. Daugherty, N. van Bruggen, H.P. Redmond, R.A. Carano, E.H. Filvaroff, Vascular endothelial growth factor stimulates bone repair by promoting angiogenesis and boneturnover, Proc. Natl. Acad. Sci. U. S. A. 99 (15) (2002 Jul 23) 9656–9661.
[4] T. Matsumoto, G.M. Cooper, B. Gharaibeh, L.B. Meszaros, G. Li, A. Usas, F.H. Fu, J. Huard, Blocking VEGF as a potential approach to improve cartilage healing after osteoarthritis, J. Musculoskelet. Neuronal Interact. 8 (4) (2008 Oct-Dec) 316–317.
[5] M. Giacca, S. Zacchigna, VEGF gene therapy: therapeutic angiogenesis in the clinic and beyond, Gene Ther. 19 (6) (2012 Jun) 622–629.
[6] R.E. Unger, E. Dohle, C.J. Kirkpatrick, Improving vascularization of engineered bone through the generation of pro-angiogenic effects in co-culture systems, Adv. Drug Deliv. Rev. 94 (2015 Nov 1) 116–125.
[7] E. Dohle, I. Bischoff, T. Böse, A. Marsano, A. Banfi, R.E. Unger, C.J. Kirkpatrick, Macrophage-mediated angiogenic activation of outgrowth endothelial cells in co-culture with primary osteoblasts, Eur. Cell Mater 27 (149–64) (2014 Feb 19) discussion 164–5.
[8] U. Bulnheim, P. Müller, H.G. Neumann, K. Peters, R.E. Unger, C.J. Kirkpatrick, J. Rychly, Endothelial cells stimulate osteogenic differentiation of mesenchymal stem cells on calcium phosphate scaffolds, J. Tissue Eng. Regen. Med. 8 (10) (2014 Oct) 831–840.
[9] S. Ghanaati, R.E. Unger, M.J. Webber, M. Barbeck, C. Orth, J.A. Kirkpatrick, P. Booms, A. Motta, C. Migliaresi, R.A. Sader, C.J. Kirkpatrick, Scaffold vascularization in vivo driven by primary human osteoblasts in concert with host inflammatory cells, Biomaterials 32 (32) (2011 Nov) 8150–8160.
[10] R.E. Unger, S. Ghanaati, C. Orth, A. Sartoris, M. Barbeck, S. Halstenberg, A. Motta, C. Migliaresi, C.J. Kirkpatrick, The rapid anastomosis between prevascularized networks on silk fibroin scaffolds generated in vitro with cocultures of human microvascular endothelial and osteoblast cells and the host vasculature, Biomaterials 31 (27) (2010 Sep) 6959–6967.
[11] M.K. Boushell, C.T. Hung, E.B. Hunziker, E.J. Strauss, H.H. Lu, Current strategies for integrative cartilage repair, Connect. Tissue Res. (2016 Sep 6) 1–14.
[12] A. Lindahl, M. Brittberg, L. Peterson, Cartilage repair with chondrocytes: clinical and cellular aspects, Novartis Found. Symp. 249 (175–86) (2003) discussion 186-9, 234-8, 239-41.
[13] C. Brochhausen, N. Sánchez, S. Halstenberg, R. Zehbe, B. Watzer, V.H. Schmitt, A. Hofmann, A. Meurer, R.E. Unger, C.J. Kirkpatrick, Phenotypic redifferentiation and cell cluster formation of cultured human articular chondrocytes in a three-dimensional oriented gelatin scaffold in the presence of PGE2—first results of a pilot study, J. Biomed. Mater Res. A 101 (8) (2013 Aug) 2374–2382.
[14] A. Marsano, C.M. Medeiros da Cunha, S. Ghanaati, S. Gueven, M. Centola, R. Tsaryk, M. Barbeck, C. Stuedle, A. Barbero, U. Helmrich, S. Schaeren, J.C. Kirkpatrick, A. Banfi, I. Martin, Spontaneous in vivo chondrogenesis of bone marrow-derived mesenchymal progenitor cells by blocking vascular endothelial growth factor signaling, Stem Cells Transl. Med. 5 (12) (2016 Dec) 1730–1738.
[15] J.M. Anderson, A. Rodriguez, D.T. Chang, Foreign body reaction to biomaterials, Semin. Immunol. 20 (2) (2008) 86–100.
[16] S. Ghanaati, M. Barbeck, C. Orth, I. Willershausen, B.W. Thimm, C. Hoffmann, A. Rasic, R.A. Sader, R.E. Unger, F. Peters, C.J. Kirkpatrick, Influence of β-tricalcium phosphate granule size and morphology on tissue reaction in vivo, Acta Biomater. 6 (12) (2010) 4476–4487.
[17] D. Le Nihouannen, L.L. Guehennec, T. Rouillon, P. Pilet, M. Bilban, P. Layrolle, G. Daculsi, Micro-architecture of calcium phosphate granules and fibrin glue composites for bone tissue engineering, Biomaterials 27 (13) (2006) 2716–2722.
[18] S.M. Ghanaati, B.W. Thimm, R.E. Unger, C. Orth, T. Kohler, M. Barbeck, R. Müller, C.J. Kirkpatrick, Collagen-embedded hydroxylapatite–beta-tricalcium phosphate–silicon dioxide bone substitute granules assist rapid vascularization and promote cell growth, Biomed. Mater 5 (2) (2010 Apr) 25004.
[19] S. Ghanaati, M. Barbeck, R. Detsch, U. Deisinger, U. Hilbig, V. Rausch, R. Sader, R.E. Unger, G. Ziegler, C.J. Kirkpatrick, The chemical composition of synthetic bone substitutes influences tissue reactions in vivo: histological and histomorphometrical analysis of the cellular inflammatory response to hydroxyapatite, beta-tricalcium phosphate and biphasic calcium phosphate ceramics, Biomed. Mater 7 (1) (2012) 015005.
[20] S. Ghanaati, M. Barbeck, U. Hilbig, C. Hoffmann, R.E. Unger, R.A. Sader, F. Peters, C.J. Kirkpatrick, An injectable bone substitute composed of beta-tricalcium phosphate granules, methylcellulose and hyaluronic acid inhibits connective tissue influx into its implantation bed in vivo, Acta Biomater. 7 (11) (2011) 4018–4028.
[21] B.N. Brown, B.D. Ratner, S.B. Goodman, S. Amar, S.F. Badylak, Macrophage polarization: an opportunity for improved outcomes in biomaterials and regenerative medicine, Biomaterials 33 (15) (2012) 3792–3802.
[22] M. Barbeck, P. Booms, R. Unger, V. Hoffmann, R. Sader, C.J. Kirkpatrick, S. Ghanaati, Multinucleated giant cells in the implant bed of bone substitutes are foreign body giant cells-New insights into the material-mediated healing process, J. Biomed. Mater Res. A 104 (12) (2016 Dec) 2928–2935.
[23] M. Barbeck, A. Motta, C. Migliaresi, R. Sader, C.J. Kirkpatrick, S. Ghanaati, Heterogeneity of biomaterial-induced multinucleated giant cells: possible importance for the regeneration process? J. Biomed. Mater Res. A 104 (2) (2016 Feb) 413–418.
[24] P. Lichte, H.C. Pape, T. Pufe, P. Kobbe, H. Fischer, Scaffolds for bone healing: concepts, materials and evidence, Injury 42 (6) (2011) 569–573.
[25] T. Serra, J.A. Planell, M. Navarro, High-resolution PLA-based composite scaffolds via 3-D printing technology, Acta Biomater. 9 (3) (2013 Mar) 5521–5530.
[26] D.E. Cutright, E.E. Hunsuck, Tissue reaction to the biodegradable polylactic acid suture, Oral Surg. Oral Med. Oral Pathol. 31 (1) (1971 Jan) 134–139.
[27] Y. Ramot, M. Haim-Zada, A.J. Domb, A. Nyska, Biocompatibility and safety of PLA and its copolymers, Adv. Drug Deliv. Rev. 107 (2016 Dec 15) 153–162.
[28] K. Rezwan, Q.Z. Chen, J.J. Blaker, A.R. Boccaccini, Biodegradable and bioactive porous polymer/inorganic composite scaffolds for bone tissue engineering, Biomaterials 27 (18) (2006) 3413–3431.
[29] A. Aguirre, A. Gonzalez, M. Navarro, O. Castaño, J.A. Planell, E. Engel, Control of microenvironmental cues with a smart biomaterial composite promotes endothelial progenitor cell angiogenesis, Eur. Cell Mater 24 (2012) 90–106 discussion 106.
[30] O.F. Vila, J.R. Bag, M. Navarro, M. Alieva, E. Aguilar, E. Engel, J.A. Planell, N. Rubio, J. Blanco, Calcium phosphate glass improves angiogenesis capacity of poly(lactic acid) scaffolds and stimulates differentiation of adipose tissue-derived mesenchymal stromal cells to the endothelial lineage, J. Biomed. Mater Res. A 101 (2013) 932–941.
[31] Alejandro A. Gorustovich, Judith A. Roether, Aldo R. Boccaccini, Effect of bioactive glasses on angiogenesis: a review of in vitro and in vivo evidences, Tissue Eng. Part B Rev. 16 (2) (April 2010) 199–207.
[32] M. Charles-Harris, M.A. Koch, M. Navarro, D. Lacroix, E. Engel, J.A. Planell, A PLA/calcium phosphate degradable composite material for bone tissue engineering: an in vitro study, J. Mater Sci. Mater Med. 19 (2008) 1503–1513.
[33] M. Vogel, C. Voigt, C. Knabe, R.J. Radlanski, U.M. Gross, C.M. Müller-Mai, Development of multinuclear giant cells during the degradation of Bioglass particles in rabbits, J. Biomed. Mater Res. A 70 (3) (2004 Sep 1) 370–379.
[34] M. Barbeck, M. Dard, M. Kokkinopoulou, J. Markl, P. Booms, R.A. Sader, C.J. Kirkpatrick, S. Ghanaati, Small-sized granules of biphasic bone substitutes support fast implant bed vascularization, Biomatter (2015 Jun 17) 0.
[35] M. Barbeck, S.E. Udeabor, J. Lorenz, A. Kubesch, J. Choukroun, R.A. Sader, C.J. Kirkpatrick, S. Ghanaati, Induction of multinucleated giant cells in response to small sized bovine bone substitute (Bio-Oss™) results in an enhanced early implantation bed vascularization, Ann. Maxillofac. Surg. 4 (2) (2014 Jul-Dec) 150–157.
[36] M. Barbeck, S. Udeabor, J. Lorenz, M. Schlee, M. Grosse Holthaus, N. Raetscho, J. Choukroun, R. Sader, C.J. Kirkpatrick, S. Ghanaati, High-temperature sintering of xenogeneic bone substitutes leads to increased multinucleated giant cell formation: in vivo and preliminary clinical results, J. Oral Implantol. 41 (5) (2015 Oct) e212–22.
[37] M. Barbeck, J. Lorenz, M. Grosse Holthaus, N. Raetscho, A. Kubesch, P. Booms, R. Sader, C.J. Kirkpatrick, S. Ghanaati, Porcine dermis and pericardium-based, non cross-linked materials induce multinucleated giant cells after their in vivo implantation: a physiological reaction? J. Oral Implantol. (2014).
[38] M. Barbeck, J. Lorenz, A. Kubesch, P. Booms, N. Boehm, J. Choukroun, R. Sader, C.J. Kirkpatrick, S. Ghanaati, Porcine dermis-derived collagen membranes induce implantation bed vascularization via multinucleated giant cells: a physiological reaction? J. Oral Implantol. (2014).
[39] T. Serra, M. Ortiz-Hernandez, E. Engel, J.A. Planell, M. Navarro, Relevance of PEG in PLA-based blends for tissue engineering 3D-printed scaffolds, Mater Sci. Eng. C Mater Biol. Appl. 38 (2014 May 1) 55–62.
[40] M. Navarro, M.P. Ginebra, J.A. Planell, Cellular response to calcium phosphate glasses with controlled solubility, J. Biomed. Mater Res. A 67 (3) (2003 Dec 1) 1009–1015.
[41] S.S. Liao, F.Z. Cui, In vitro and in vivo degradation of mineralized collagen-based composite scaffold: nanohydroxyapatite/collagen/poly(L-lactide), Tissue Eng. 10 (2004) 73–80.
[42] E. Saito, Y. Liu, F. Migneco, S.J. Hollister, Strut size and surface area effects on long-term in vivo degradation in computer designed poly(L-lactic acid) three-dimensional porous scaffolds, Acta Biomater. 8 (7) (2012 Jul) 2568–2577.
[43] M. Navarro, M.P. Ginebra, J.A. Planell, C.C. Barrias, M.A. Barbosa, In vitro degradation behavior of a novel bioresorbable composite material based on PLA and a soluble CaP glass, Acta Biomater. 1 (4) (2005 Jul) 411–419.
[44] H. Zhou, J.G. Lawrence, S.B. Bhaduri, Fabrication aspects of PLA-CaP/PLGA-CaP composites for orthopedic applications: a review, Acta Biomater. 8 (6) (2012 Jul) 1999–2016.
[45] D.W. Hutmacher, J.T. Schantz, C.X. Lam, K.C. Tan, T.C. Lim, State of the art and future directions of scaffold-based bone engineering from a biomaterials

perspective, J. Tissue Eng. Regen. Med. 1 (4) (2007 Jul-Aug) 245–260.
[46] A. Aguirre, A. González, J.A. Planell, E. Engel, Extracellular calcium modulates in vitro bone marrow-derived Flk-1+ CD34+ progenitor cell chemotaxis and differentiation through a calcium-sensing receptor, Biochem. Biophys. Res. Commun. 393 (1) (2010) 156–161.
[47] M. Barbeck, S. Najman, S. Stojanović, Živković JM. Mitić Ž, J. Choukroun, P. Kovačević, R. Sader, C.J. Kirkpatrick, S. Ghanaati, Addition of blood to a phycogenic bone substitute leads to increased in vivo vascularization, Biomed. Mater 10 (5) (2015 Sep 11) 055007.
[48] A.K. McNally, J.M. Anderson, Multinucleated giant cell formation exhibits features of phagocytosis with participation of the endoplasmic reticulum, Exp. Mol. Pathol. 79 (2) (2005 Oct) 126–135.
[49] G.D. Roodman, Cell biology of the osteoclast, Exp. Hematol. 27 (8) (1999) 1229–1241.
[50] G.W. Oddie, G. Schenk, N.Z. Angel, N. Walsh, L.W. Guddat, J. de Jersey, A.I. Cassady, S.E. Hamilton, D.A. Hume, Structure, function, and regulation of tartrate-resistant acid phosphatase, Bone 27 (5) (2000 Nov) 575–584.
[51] C.J. Wilson, R.E. Clegg, D.I. Leavesley, M.J. Pearcy, Mediation of biomaterial-cell interactions by adsorbed proteins: a review, Tissue Eng. 11 (1–2) (2005 Jan-Feb) 1–18.
[52] L. Tang, T.P. Ugarova, E.F. Plow, J.W. Eaton, Molecular determinants of acute inflammatory responses to biomaterials, J. Clin. Invest. 97 (5) (1996) 1329–1334.
[53] L. Tang, Mechanisms of fibrinogen domains: biomaterial interactions, J. Biomater. Sci. Polym. Ed. 9 (12) (1998) 1257–1266.
[54] J.M. Anderson, Biological responses to materials, Annu. Rev. Mater Res. 31 (2001) 81–110.
[55] M. Jayaraman, U. Meyer, M. Bühner, U. Joos, H.P. Wiesmann, Influence of titanium surfaces on attachment of osteoblast-like cells in vitro, Biomaterials 25 (4) (2004) 625–631.